Editors' Suggestion

Tracking the evolution from isolated dimers to many-body entanglement in $NaLu_xYb_{1-x}Se_2$

Luke Pritchard Cairns,[1,2,*] Ryan Day,[1,2] Shannon Haley,[1,2] Nikola Maksimovic,[1,2] Josue Rodriguez,[1,2] Hossein Taghinejad,[1] John Singleton,[3] and James Analytis[1,2,4]

[1]*Department of Physics, University of California, Berkeley, California 94720, USA*

[2]*Materials Science Division, Lawrence Berkeley National Laboratory, Berkeley, California 94720, USA*

[3]*National High Magnetic Field Laboratory, Los Alamos National Laboratory, Los Alamos, New Mexico 87545, USA*

[4]*CIFAR Quantum Materials, CIFAR, Toronto, Canada*

(Received 1 April 2022; revised 5 June 2022; accepted 6 June 2022; published 7 July 2022)

We synthesize homogeneous compositions of $NaLu_xYb_{1-x}Se_2$, connecting nonmagnetic $NaLuSe_2$ to the triangular lattice spin liquid candidate $NaYbSe_2$. Thermal and magnetic properties are studied as the system evolves from one with dilute magnetic defects to one of a dense magnetic lattice. The field- and temperature-dependent heat capacity show the carriers of entropy cross over from isolated magnetic ions to a correlated lattice born from spin dimers. For the dilute system we estimate the single-ion anisotropy ($g_\perp/g_\parallel = 3.13$) and also the dimer exchange couplings $J_\parallel$ (=5.4 K) and $J_\perp$ (=9.6 K), in order to draw comparison to the half-doped and full magnetic compounds.

DOI: 10.1103/PhysRevB.106.024404

I. INTRODUCTION

A quantum spin liquid (QSL) is a theoretical construct wherein a system of strongly interacting localized moments shows no magnetic order but instead forms a massively entangled state, in some cases giving rise to fractionalized, dispersive excitations [1–3]. A material's QSL candidacy often begins with a magnetic lattice that conforms to some known model. For instance, the triangular lattice antiferromagnet (TLAF) plays host to a variety of QSL states [4–8], all of which rely on some form of anisotropic exchange or next-nearest-neighbor interactions [9]. The candidate material should then exhibit no long-range order (or spin freezing) in spite of strong magnetic correlations, and finally, show some definitive, positive experimental signature of QSL physics. For example, a finite residual linear term in the heat capacity or thermal conductivity [10,11], a broad spectrum of low-energy excitations observed via neutron scattering [12,13], or a quantized thermal Hall conductivity [14] have all previously been taken as evidence. Unfortunately however, at present, the most promising candidate materials remain subject to debate [15–19].

$NaYbSe_2$ is one such candidate QSL material. It belongs to a recently discovered class of Yb delafossites [20,21], and comprises alternating planes of distorted $YbSe_6$ and $NaSe_6$ octahedra [as shown in the inset of Fig. 1(a)]. A combination of spin-orbit coupling and crystalline electric field (CEF) gradients split the Yb^{3+} $4f^{13}$ energy levels into seven Kramers doublets, the lowest of which is separated from the first excited state by ∼180 K [22]. At low temperatures the Yb^{3+} ions are therefore confined to the doubly degenerate ground state, and can be modeled as pseudospin-1/2 moments [23]. These magnetic sites make up a perfectly triangular lattice, and are coupled in an anisotropic, antiferromagnetic fashion—conforming to those anisotropic TLAF models which predict QSL states in certain pockets of parameter space [7]. Indeed, previous studies have observed a finite Sommerfeld coefficient in the specific heat [24], low-energy excitations with a V-shaped dispersion about the Γ point [25], and persistent spin fluctuations down to 50 mK [26]. Altogether this constitutes a strong case for a ground state with gapless, dispersive excitations. However—as with the majority of QSL candidates—these excitations do not appear in the low-temperature thermal conductivity [27].

We propose a divergence from the typical exploration of a QSL candidate material. By first stripping away the magnetic interactions it is possible to isolate the single-ion behavior within an identical CEF environment. Then, by steadily scaling these back up again we have the power to investigate the evolution of correlations, first in single dimers, through larger finite clusters, and building toward the full magnetic state.

In this work we have succeeded in growing $NaYbSe_2$, its nonmagnetic analog $NaLuSe_2$, and also doped $NaLu_xYb_{1-x}Se_2$, with $x = 0.5$ and 0.9. By employing a range of experimental techniques we are able to demonstrate that the doped compounds are high-quality single crystals, both of which retain the salient features of the parent compound and—crucially for any meaningful study of the evolution of correlations—comprise a homogeneous mixture of magnetic and nonmagnetic ions. The four compounds were chosen to act as, respectively, the QSL candidate material ($x = 0$), the nonmagnetic background ($x = 1$), a system at the percolation threshold ($x = 0.5$), and a system of isolated magnetic ions and small clusters ($x = 0.9$). From this, we are able to investigate the evolution of correlations as a function of magnetic cluster size via measurements of the low-temperature specific heat. We believe that $NaLu_xYb_{1-x}Se_2$ offers a new route to an understanding of similar candidate materials, in which spin-orbit coupling is leveraged as a means to generate anisotropic exchange

*lpc@berkeley.edu

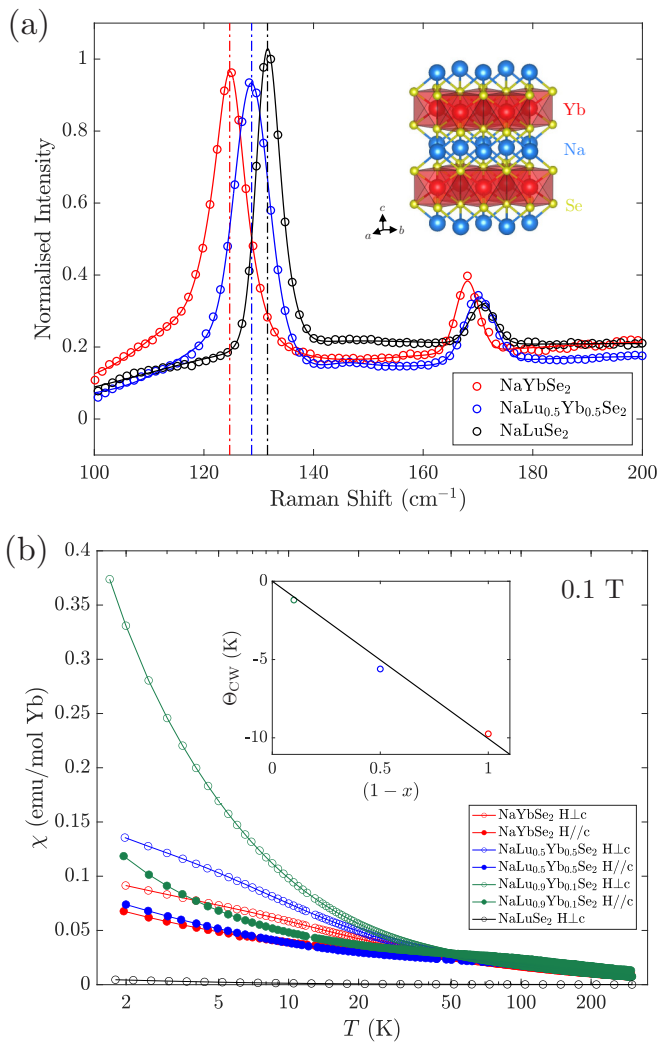

FIG. 1. (a) Raman spectra of the materials $NaLu_xYb_{1-x}Se_2$, where $x = 0$, 0.5, and 1, obtained at 300 K in all cases. The solid lines show a sum of Gaussians fitted through the data, while the dot-dash lines show the position of the E_g peak. The inset shows the crystal structure of $NaYbSe_2$ ($R\bar{3}m$, space group 166). (b) Magnetic susceptibility per mole of Yb for $NaLu_xYb_{1-x}Se_2$, where $x = 0$, 0.5, 0.9, and per mole of material for $NaLuSe_2$, plotted as a function of temperature for both in-plane and out-of-plane fields. All data were obtained in a field of 0.1 T. The inset shows the linear evolution of the Curie-Weiss temperature as a function of Yb content [estimated from fits in the region $T < 50$ K, shown in Fig. S4(a)].

interactions, but the resulting projected pseudospin basis may not simply map onto the archetypal QSL models.

II. RESULTS

Detailed descriptions of the crystal growth and experimental methods are included in the Supplemental Material [28] (SM; see also Refs. [22,24,29–32] therein).

A. Sample characterization and evidence for homogeneity

Single crystals of $NaLu_xYb_{1-x}Se_2$ (with $x = 0$, 0.5, 0.9, and 1) were grown by the flux method, following a similar procedure to previous studies [24]. Energy-dispersive x-ray (EDX) spectroscopy was employed to confirm that all four compounds are of the desired composition, while powder x-ray diffraction (PXRD) shows that all share the anticipated $R\bar{3}m$ rhombohedral structure. Further, as shown in Fig. S2, with increasing Lu content the in-plane lattice constant decreases, while the out-of-plane increases. This is typical of similar compounds containing Yb/Lu in an octahedral environment [20,33]. We note however that both techniques are essentially averaging over too large a length scale to definitively claim microscopic homogeneity, although a lack of broadening in the diffraction peaks might be taken as weak evidence.

Instead, Raman spectroscopy—which probes the E_g and A_{1g} phonon modes [22]—can effectively demonstrate homogeneity. As shown in Fig. 1(a), the peak energy of the E_g mode is $\sim$7 cm^{-1} (10 K) larger in $NaLuSe_2$ as compared to $NaYbSe_2$; this implies a stiffening of the bonds in the nonmagnetic compound. If the half-doped compound comprised separate regions of the two end compounds, we would expect two distinct E_g peaks in the Raman spectrum. Instead, we observe a single sharp peak lying almost exactly between those of the two end compounds. Considering the localized nature of the Raman vibrations, our measurements reflect the uniform intermixing of magnetic ions without a detectable elemental segregation. We note that previous studies have used Raman spectroscopy for a similar purpose [34,35].

Further evidence for microscopic homogeneity comes from the magnetization data. Figure 1(b) shows the magnetic susceptibility plotted as a function of temperature. In all cases, the zero-field- and field-cooled curves are identical. Regardless of doping, the magnetic compounds exhibit similar features for an in-plane field. At higher temperatures ($T >$ 100 K), all are well described by the Curie-Weiss law, with a Curie-Weiss temperature $\Theta_{CW} \sim 50$ K and a moment of $\sim$4.5 μ_B [as shown in Fig. S4(a)]. This is similar to the value for a Yb^{3+} free ion (=4.54 μ_B). In all cases, the trigonal CEF splits the Yb^{3+} $j = 7/2$ energy level into 4 Kramers doublets, with the first excited state being approximately 180 K above the ground state [22]. This leads to the emergence of a pseudospin-1/2 state at the lowest temperatures, wherein the Yb^{3+} ion is constrained to the ground state doublet. Strong second-order corrections complicate the analysis in this temperature regime (as discussed in the SM), but the in-plane inverse susceptibility is well fitted using a modified form of the Curie-Weiss law for $T < 50$ K (Fig. S4). Crucially, the extracted low-temperature Θ_{CW} scales linearly with Yb content [as shown in the inset of Fig. 1(b)], suggesting that the strength of the mean field at the Yb sites—and therefore the average number of magnetic nearest neighbors—scales similarly. This is the expectation for a homogeneous lattice [36]. Again, if there were instead separate macroscopic regions of the two end compounds, Θ_{CW} would remain constant.

B. $NaLu_{0.9}Yb_{0.1}Se_2$

As shown in Fig. 2(a), the magnetization of $NaLu_{0.9}Yb_{0.1}Se_2$ is highly anisotropic and fails to saturate for either field direction. For in-plane fields, the high-field magnetization is linear [as clearly demonstrated by

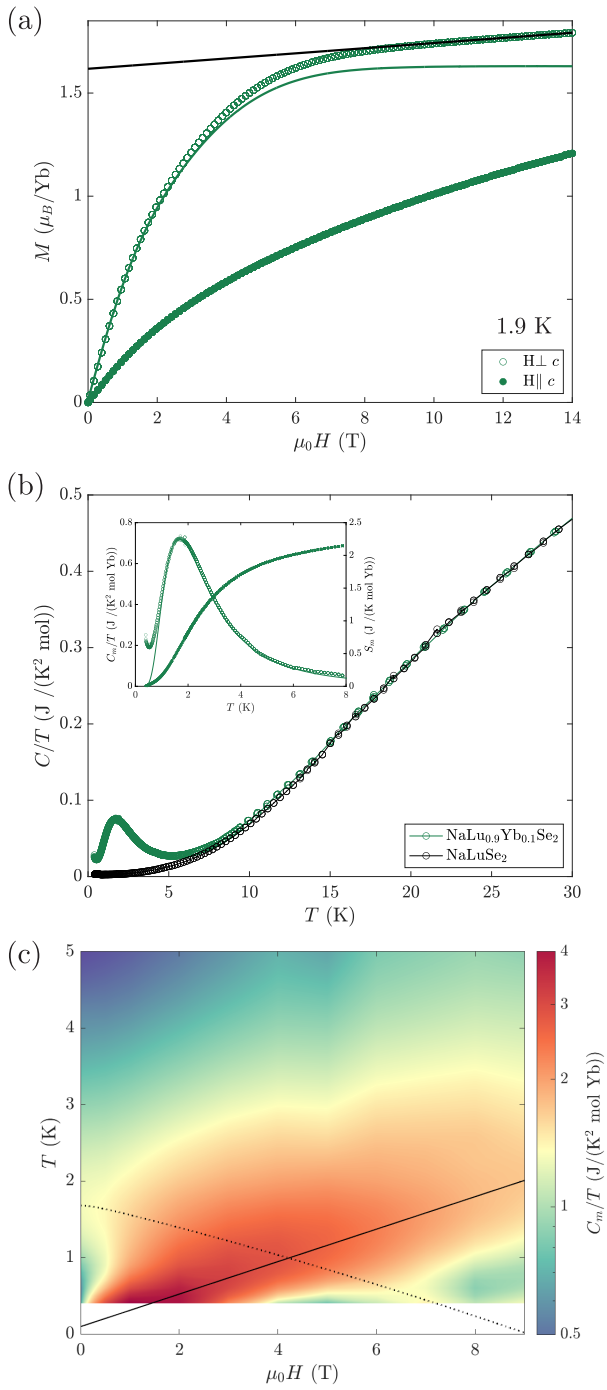

FIG. 2. (a) Magnetization as a function of field for $NaLu_{0.9}Yb_{0.1}Se_2$, plotted for both field directions. Both data sets were taken at 1.9 K. The black line shows the linear Van Vleck contribution for in-plane fields, estimated by fitting to the $H > 12$ T data. The green line shows the in-plane magnetization with this contribution subtracted. (b) Zero-field heat capacity per mole of material for $NaLu_{0.9}Yb_{0.1}Se_2$ and $NaLuSe_2$. The inset shows the magnetic heat capacity of the former, and also the released entropy. The solid line is a fit to a two-level system, with $\Delta E = 5.4$ K and 37% of the sites contributing. (c) Specific heat as a function of temperature and field for $NaLu_{0.9}Yb_{0.1}Se_2$. The applied field was out-of-plane. The solid/dotted lines show the approximate positions of the lowest-energy single ion and isolated dimer peak, respectively. The color bar is on a logarithmic scale for clarity.

differentiating the data with respect to field; Fig. S3(a)]. This is the linear Van Vleck paramagnetism—related to field-induced transitions between the CEF split levels [32]—which we estimate to be 0.0125 $\mu_B\,\mathrm{T}^{-1}$/Yb. From this, we can extract the saturation moment $M^s_\perp = 1.63\ \mu_B$/Yb, and therefore $g_\perp = 2\frac{M^s_\perp}{\mu_B} = 3.26$. This is approximately 10% larger than the in-plane g factor determined previously for the full magnetic compound [22,24,31]. A similar analysis is not possible for out-of-plane fields, as the magnetization remains nonlinear up to 14 T, and the Van Vleck contribution is not expected to be simply a small additive correction [30]. Instead, $g_\parallel$ will be estimated from a field-induced Schottky anomaly in the specific heat, as described below.

Regardless, a strong anisotropy is clearly evident. The magnetization in $NaLu_{0.9}Yb_{0.1}Se_2$ will be dominated by isolated Yb^{3+} ions, and the anisotropy is thus primarily a single-ion phenomenon. This supports the qualitative picture, wherein the prolate $4f^{13}$ quadrupolar moment is sandwiched by negative charge and therefore preferentially orients in the plane [37,38].

Figure 2(b) shows the zero-field specific heat of $NaLu_{0.9}Yb_{0.1}Se_2$, plotted alongside the nonmagnetic $NaLuSe_2$. The latter behaves as an almost ideal nonmagnetic analog, with a featureless heat capacity that roughly follows the Debye law ($\Theta_D = 259.8$ K). At the lowest temperatures there appears a small increase [see Fig. S6(b)], which we may attribute to the interaction between the Lu nuclear quadrupolar moment and the surrounding CEF gradients. Above approximately 15 K, the two compounds fall onto the same curve. We expect some excess heat capacity in the magnetic compound at higher temperatures due to thermal population of the Yb^{3+} first excited CEF level [31], but that does not affect the low-temperature behavior.

Below 10 K a peak feature develops in $NaLu_{0.9}Yb_{0.1}Se_2$. This is shown more clearly in the inset, which plots the magnetic specific heat per mole of Yb, obtained by subtracting an interpolation through the $NaLuSe_2$ data. Also included in the inset is the released entropy, which rises to 2.15 $\mathrm{J\,K^{-1}\,mol^{-1}}$ at 8 K. This is only ∼37% of the $R\ln(2)$ entropy contained within a system of spin-1/2 moments. Instructively, this is also approximately the same percentage of sites that will have one magnetic nearest neighbor in a triangular lattice at 10% filling. The observed peak is therefore likely attributable to the entropy stored in Yb dimers. As a first approximation, the peak is well fitted by a simple two-level model (shown in the figure), implying that these dimers interact via a well-defined energy scale.

In order to investigate the missing entropy, Fig. 2(c) shows the temperature-field evolution of the specific heat [the same data are also presented in Fig. S5(a) as a line plot]. With the application of field, there appears a second peak superimposed on the first, which moves to higher temperatures with increasing field. Significantly, as shown in Fig. 3(a), the total entropy change between 0.4–8 K rises almost to $R\ln(2)$ at intermediate fields, implying that nearly all of the spin-1/2 sites release their entropy within the measured temperature window. The remainder of the (nondimerized) magnetic ions must therefore contribute this second peak.

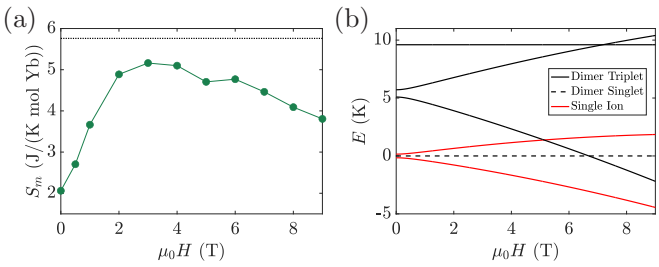

FIG. 3. (a) Entropy released by $NaLu_{0.9}Yb_{0.1}Se_2$ between 0.4–8 K, plotted as a function of field. The dotted line is at $R \ln 2$. (b) Field evolution of the energy levels for both an isolated single ion (red) and isolated dimer (black) calculated from the parameters estimated by the magnetization ($g_\parallel = 1.04$), in-field specific heat ($J_\parallel = 5.4$ K and $J_\perp = 9.6$ K), and susceptibility ($\alpha_\perp = 0.016\ \mu_B\,\mathrm{T}^{-1}$; see SM).

The field-induced peak is naturally explained by a Zeeman splitting of the Yb^{3+} ground state doublet, for which the energy splitting $\Delta = g_\parallel \mu_B H_{\mathrm{eff}}$. $H_{\mathrm{eff}} = \sqrt{H^2 + H_0^2}$, where H is the applied field and H_0 accounts for a dipolar field from neighboring ions, or possibly impurity spins [39,40]. This additional contribution is necessary to explain the zero-field splitting, which is evident from a low-temperature upturn in the zero-field data. We note that any second-order corrections to the Zeeman splitting will affect both energy levels in a similar fashion, such that the energy splitting remains linear in field.

The picture is therefore that of two noninteracting species, one of single ions and the other of dimers, each of which have an independent characteristic energy scale. In order to draw quantitative conclusions, we can attempt to model the specific heat within this framework. For the most general discretized system—having n levels, each with an energy E_n and degeneracy g_n—the specific heat is given by

$$C(T) = R\frac{d}{dT}\left[\frac{\sum_n g_n E_n e^{-E_n/k_B T}}{\sum_n g_n e^{-E_n/k_B T}}\right], \tag{1}$$

which in the case of a Zeeman-split doublet reduces to

$$C(T) = R\left(\frac{\Delta}{T}\right)^2 \frac{e^{-\Delta/T}}{(1+e^{-\Delta/T})^2}, \tag{2}$$

where the energy splitting Δ is given above (and expressed here in kelvins). This function has a maximum at a temperature of 0.42Δ, and the field evolution of the specific heat can therefore be used to determine the out-of-plane g factor. Figure 2(c) shows a linear fit through the peak, from which we estimate $g_\parallel = 1.04$ [the same linear fit is shown more clearly in the inset of Fig. S5(a)]. Together with $g_\perp = 3.26$ estimated from the magnetization data, we calculate an easy-plane anisotropy of 3.13. This is similar to (but slightly larger than) the easy-plane anisotropy estimated for the full magnetic compound [22,24,31].

In order to model the remainder of the magnetic ions, we treat them as a system of isolated dimers. For a single dimer, the four possible states can be expressed $|S, s_z\rangle$, where S is the total effective spin and s_z is the projection of this spin along the quantization axis. For an isotropic antiferromagnetic exchange interaction, the ground state singlet ($|0,0\rangle$) will be separated from the degenerate triplet ($|1,-1\rangle$, $|1,0\rangle$, and $|1,1\rangle$) by an energy proportional to the strength of exchange. However, in the case of anisotropic exchange, the triplet level will in general be split. For example, consider anisotropic exchange described by the Hamiltonian

$$\mathcal{H} = J_\perp\left(S_1^x S_2^x + S_1^y S_2^y\right) + J_\parallel S_1^z S_2^z, \tag{3}$$

or the XXZ model. In this scenario, the $|1,0\rangle$ state will be separated from the ground state singlet by an energy $J_\perp$, whereas the $|1,\pm1\rangle$ doublet will be separated by $J_\parallel$. Crucially, an applied field H will act to shift the energies by $-g s_z \mu_B H$, implying that the $|1,\pm1\rangle$ doublet will be split, but the other energy levels will stay constant. In principle therefore, the field evolution of the specific heat can be used to determine the strength, sign, and anisotropy of the dimer exchange interaction.

We now apply this analysis to $NaLu_{0.9}Yb_{0.1}Se_2$. We model the isolated dimers as above, and also include an independent population of isolated single ions. The fitting function is discussed in the SM, but derives from Eq. (1), with the various energy levels defined by $g_\parallel$ (which we assume to be similar for both species), $J_\perp$, $J_\parallel$, and also the applied field. Higher-order corrections to the Zeeman splitting are somewhat relevant here, and lead to nonlinear, asymmetric splitting of the triplet $|1,\pm1\rangle$ level.

If we estimate the relative populations from the released entropy (at ∼37% and ∼59%, respectively), this leaves only $J_\perp$ and $J_\parallel$ to be determined. However, certain aspects of the data can help to put constraints on these. For example, the position of the peak in the zero-field specific heat implies that the lowest energy splitting of the dimer subsystem is approximately 5 K without an applied field. Further, the observed low-temperature upturn at higher fields [and corresponding decrease of released entropy within the measured temperature window; Fig. 3(a)] implies there should be a small energy splitting at high fields. This can only arise due to a crossing of the Zeeman-shifted $|1,1\rangle$ state and the singlet ground state [as shown more clearly in Fig. 3(b)]. Given $g_\parallel = 1.04$, the $|1,1\rangle$ level must be at ∼5 K in zero field in order to give the observed upturn at higher fields. This naturally accounts for the zero-field peak, and implies that $|1,\pm1\rangle$ is the first excited state.

Fitting to the zero-field data gives $J_\parallel = 5.4$ K and $J_\perp = 9.6$ K, although the latter is significantly less well constrained as the smaller energy splittings dominate the specific heat. The field evolution of the isolated ion and dimer energy levels is shown Fig. 3(b). This model is able to reproduce the essential features of the in-field specific heat data, as shown in Fig. S5(b). The magnitudes of the exchange couplings are slightly larger than those estimated for the full magnetic compound (via fits to the low-temperature susceptibility [24,31]), but of the same order and proportionality, and with the same hierarchy.

We note that there may be some additional complications to the above model. For example, this framework does not account for larger magnetic clusters, although the released entropy alongside the adequacy of the zero-field fitting would suggest that these are insignificant. Also, there may be relevant anisotropic exchange terms beyond the

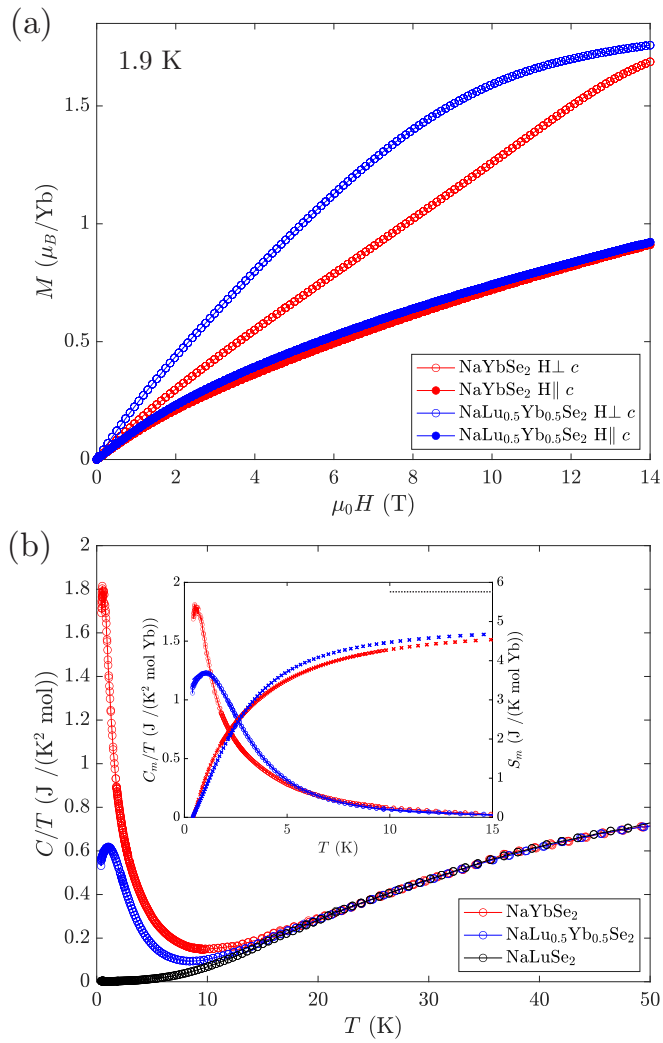

FIG. 4. (a) Magnetization of $NaLu_{0.5}Yb_{0.5}Se_2$ and $NaYbSe_2$ as a function of field, taken at 1.9 K in both cases. (b) Zero-field specific heat of both compounds, compared to the nonmagnetic analog $NaLuSe_2$. The inset shows the magnetic specific heat and also the released entropy. The solid blue line is a fit of the $NaLu_{0.5}Yb_{0.5}Se_2$ data to a Gaussian broadened two-level system, and the dashed black line is at $R \ln 2$, the upper bound for a spin-1/2 system.

XXZ model, but previous studies disagree on whether these should be negligible in comparison [23,31]. Finally, the field evolution will necessarily be impacted by second-order corrections to the Zeeman splitting. The strength of these corrections has been determined by fitting to the susceptibility (Fig. S4), but this appears to give a slight underestimation as compared to the same correction extracted from the magnetization (although it is only possible to draw comparison in one case).

C. $NaLu_{0.5}Yb_{0.5}Se_2$ and $NaYbSe_2$

The data for $NaLu_{0.5}Yb_{0.5}Se_2$ and $NaYbSe_2$ are largely similar, and it seems sensible to discuss them in tandem. Figure 4(a) shows the magnetization. Both compounds retain a strong anisotropy, and neither approaches linearity at high fields. In fact, as demonstrated in Fig. S3(b), the out-of-plane magnetization in $NaLu_{0.5}Yb_{0.5}Se_2$ fails to saturate even for fields as large as 40 T. Similar to $NaLu_{0.9}Yb_{0.1}Se_2$, this would imply that the Van Vleck contribution is not simply a negligible addition, and must be determined via a different means (for example by fitting to the susceptibility, as shown in Fig. S4). Without saturation it is difficult to be quantitative, but it is perhaps interesting that the low-field anisotropy falls with increasing Yb content, suggesting that the single-ion anisotropy is potentially mitigated.

As with $NaLu_{0.9}Yb_{0.1}Se_2$, the zero-field specific heat [shown in Fig. 4(b)] of both compounds exhibits a low-temperature peak, before falling onto the $NaLuSe_2$ curve above 20 K. In this case however, the magnetic specific heat cannot be fitted using a simple two-level model. Instead, a "best" fit to the $NaLu_{0.5}Yb_{0.5}Se_2$ data [shown in the inset of Fig. 4(b)] requires a significant Gaussian broadening of the two-level system, although with a similar energy splitting (∼5 K) to the sharp two-level description of $NaLu_{0.9}Yb_{0.1}Se_2$. This implies that the isolated dimer model is no longer relevant, and may reflect a smearing of the relevant energy scale. The $NaYbSe_2$ peak cannot be interpreted within any similar framework, perhaps suggesting that the idea of discretized energy levels is no longer applicable. In both cases however, almost the full anticipated $R \ln 2$ entropy is released over the measured temperature window [also shown in the inset of Fig. 4(b)], and the majority of magnetic sites must therefore contribute to the low-temperature peak.

The number of isolated ions can once again be estimated from the in-field specific heat data (Fig. S5). For $NaLu_{0.5}Yb_{0.5}Se_2$, there appears a field-induced Schottky anomaly at low temperatures. However, this feature releases only an additional $0.05R \ln 2$ of entropy, corresponding to 5% of the magnetic ions being essentially uncorrelated. A simple calculation would suggest that only 1.5% should be without a magnetic nearest neighbor, but the number of effective single ions might be increased due to disorder (induced via Na substitution at the magnetic sites or excess Se, as implied by EDX measurements). Similarly to the zero-field data, the field evolution can be roughly fitted by considering that ∼90% of the sites participate in a significantly Gaussian-broadened two-level system, while ∼5% remain as isolated single ions, and are therefore Zeeman split. The remaining 5% can be accounted for again due to the excess Na and Se, which might result in a slight overestimation of the number of moles of magnetic ions.

The in-field data for $NaYbSe_2$ are likewise intractable-Fig. S5(d), but appear to evolve in a similar manner, with an increasing energy scale and broadening of the peak. Any quantitative analysis is further confused by a third peak at higher fields, which has been interpreted previously as the onset of antiferromagnetic order [24]. Importantly however, the small size of the field-induced Schottky anomaly in $NaLu_{0.5}Yb_{0.5}Se_2$ (and the absence of one in $NaYbSe_2$) would imply that in both compounds the overwhelming majority of sites are not interacting with the field in the way that a single ion might. Further, the broadening of the energy scale in $NaLu_{0.5}Yb_{0.5}Se_2$, and the absence of a significant low-temperature upturn at higher fields in either (as observed in

$NaLu_{0.9}Yb_{0.1}Se_2$), would imply that neither compound can be described as a system of isolated dimers.

III. DISCUSSION

An anomalous peak in the zero-field specific heat is a universal feature of frustrated systems that exhibit no magnetic order. Similar features have been observed to occur regardless of the nature of the spinful object [41–44], magnetic structure [45], or even dimensionality [46]. The anomalous peak in $NaYbSe_2$ has variously been interpreted as arising due to strong spin fluctuations [31], correlations between quasistatic spins [27], or simply as a consequence of the TLAF fully frustrated, disordered ground state [24]. In fact, almost any disordered ground state will result in a specific heat which rises from zero temperature and falls with a $1/T^2$ dependence at higher temperatures, such that a peak is a fairly generic feature, and the vast majority of interpretations are compatible with this observation. The peak position will invariably give some measure of the strength of correlations, but in order to obtain real insight it is often necessary to track the evolution of the specific heat under some perturbation. For example, the application of field should immediately reveal any uncorrelated spins via the emergence of an additional Schottky peak. The fact that this is absent in $NaYbSe_2$ already implies that all of the spins are participating in some form of correlated state.

An alternative method of perturbing the system is through doping [47], which in principle allows a tuning of the magnetic correlations. While doping might introduce appreciable disorder, we note that this is not necessarily an anathema to the QSL state [45,48]. Upon doping $NaYbSe_2$, the anomalous zero-field peak evolves into a well-characterized two-level Schottky peak in the dilute system ($NaLu_{0.9}Yb_{0.1}Se_2$). We have demonstrated that this feature can be entirely attributed to isolated dimers, and therefore defines the relevant energy scale for singlet formation. Nearest-neighbor interactions should not change significantly with doping, and indeed, this energy scale remains relevant in the half-doped compound. In this case however the feature is broadened, perhaps signaling the emergence of a random singlet phase. This phase can be induced by disorder—or pertinently, site dilution [49]—and is characterized by a combination of orphan spins, isolated singlet dimers, and also clusters of resonating singlet dimers, each of which interacts via a different energy scale [50]. Further, the random singlet phase has been predicted to mimic the signatures of some QSL states [17], despite it being a simple product state. For example, the low-energy excitations—such as singlet pair breaking or diffusive orphan spins—can give a T-linear low-temperature specific heat, or even a T-linear thermal conductivity. An observation of the latter in the half-doped compound would certainly be revealing, as $NaYbSe_2$ exhibits no such behavior [27].

Finally, the slightly reduced temperature of the peak in the half-doped compound as compared to $NaLu_{0.9}Yb_{0.1}Se_2$ might imply that larger-sized clusters interact on a reduced energy scale. This would naturally explain why the peak in the full magnetic compound occurs at a lower temperature still. However, it is clear that the absence of a singlet peak (sharp or broadened) in $NaYbSe_2$ suggests that the interactions have evolved beyond twosite correlations (Fig. 5), and perhaps even that we may preclude the possibility of a random singlet phase.

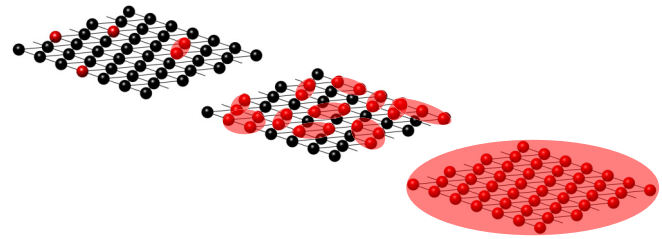

FIG. 5. Schematic to show the proposed evolution of correlations as a function of doping in $NaLu_xYb_{1-x}Se_2$, from isolated single ions and dimers ($x = 0.9$, left), through larger, finite magnetic clusters at the percolation threshold ($x = 0.5$, middle), to the full magnetic, many-body entangled state ($x = 0$, right).

From the analysis of $NaLu_{0.9}Yb_{0.1}Se_2$, we are in a position to be more quantitative. First, the easy-plane anisotropy is found to be slightly enhanced as compared to the full magnetic compound (3.13 compared to ∼3 [22,24,31]). This implies that the anisotropy observed in $NaYbSe_2$ is primarily a single-ion phenomenon, but also that it is suppressed by increasing the average number of Yb nearest neighbors. The single-ion anisotropy is driven by the surrounding CEF gradients [38], and it seems likely therefore that this suppression is due to the different charge distributions of Lu^{3+} and Yb^{3+}. In an octahedrally coordinated environment, Yb^{3+} is expected to have a slightly larger ionic radius [51]. This would act to force the prolate $4f^{13}$ quadrupolar moment out of the plane, and hence suppress the easy-plane anisotropy [37].

From the field evolution of the specific heat we have also estimated the pseudospin-1/2 dimer exchange constants $J_\parallel$ (=5.4 K) and $J_\perp$ (=9.6 K). These are slightly larger than those estimated for $NaYbSe_2$ [24,31]. This may be due to the frustration present in the full magnetic compound, or perhaps the simplifying assumptions of our model. However, unlike the magnetic susceptibility, the specific heat more directly reflects the energy spectrum, and should therefore be an accurate tool in determining the various energy scales. In refining this technique, it may be more fruitful to investigate lower dopings—wherein the impact of larger clusters can safely be disregarded—or in-plane fields—for which the second-order corrections to the Zeeman splitting are smaller, and the data might therefore be more amenable to analysis.

Finally, and perhaps ominously, we note that the singlet ground state of an isolated dimer is nonmagnetic. We should therefore expect a reduction of the magnetic susceptibility below a temperature of the order of the exchange coupling. However we observe no divergence from paramagnetic behavior, even when the susceptibility is measured at a significantly smaller field [Fig. S4(c)]. This may be due to single ions dominating the susceptibility—although a ∼35% decrease should still be observable—or perhaps due to orphan spins induced by disorder [52], which can act to enhance the susceptibility at low temperatures [53]. Alternatively, symmetry-allowed pseudodipolar interactions may mix the singlet and triplet states, resulting in a magnetic ground state. However, this effect should be negligible [23,40], and also the simplified model employed here has been successful in previous studies of Yb dimer systems [54].

We have demonstrated that $NaLu_xYb_{1-x}Se_2$ represents the ideal framework for understanding a recently discovered class of candidate spin liquid materials. The compounds are straightforward to grow, share similar characteristics across the full doping range, have an ideal nonmagnetic analog, and comprise a homogeneous mixture of magnetic and nonmagnetic ions. This allows us to track the evolution of spin correlations from isolated dimers through small entangled clusters up to the many-body entangled state in the full magnetic compound. Such an evolution opens up the possibility of studying percolation transitions in QSL candidate materials.

Note added. Recently we became aware of [55], which reports the synthesis and characterization of a related compound, $NaYb_{1-x}Lu_xS_2$. We would like to thank Ehud Altman and Chunxiao Liu for some enlightening discussions.

ACKNOWLEDGMENTS

This work was supported by the U.S. Department of Energy, Office of Science, Basic Energy Sciences, Materials Sciences and Engineering Division, under Contract No. DE-AC02-05-CH11231 within the Quantum Materials program (KC2202). Work performed by N.M. was supported by the U.S. Department of Energy, Office of Science, Office of Basic Energy Sciences, Materials Sciences and Engineering Division, under Contract No. DE-AC02-05-CH11231, within the Quantum Systems Accelerator Program. R.D. is currently supported by the Canadian Government under a Banting Fellowship. S.H. was supported as part of the Center for Novel Pathways to Quantum Coherence in Materials, an Energy Frontier Research Center funded by the United States Department of Energy, Office of Science, Basic Energy Sciences. J.R. was supported by the National Science Foundation through Award No. DMR-1905397. H.T. was supported by the EPiQS Initiative of the Gordon and Betty Moore Foundation through Grant No. GBMF9067. A portion of this work was performed at the National High Magnetic Field Laboratory (NHMFL), which is supported by National Science Foundation Cooperative Agreement No. DMR-1644779, the State of Florida, and the Department of Energy (DOE). J.S. acknowledges support from the DOE BES program "Science of 100 T."

[1] L. Savary and L. Balents, Rep. Prog. Phys. **80**, 016502 (2017).
[2] Y. Zhou, K. Kanoda, and T.-K. Ng, Rev. Mod. Phys. **89**, 025003 (2017).
[3] C. Broholm, R. J. Cava, S. A. Kivelson, D. G. Nocera, M. R. Norman, and T. Senthil, Science **367**, eaay0668 (2020).
[4] S. Sachdev, Phys. Rev. B **45**, 12377 (1992).
[5] R. Moessner and S. L. Sondhi, Phys. Rev. Lett. **86**, 1881 (2001).
[6] Z. Zhu and S. R. White, Phys. Rev. B **92**, 041105(R) (2015).
[7] Z. Zhu, P. A. Maksimov, S. R. White, and A. L. Chernyshev, Phys. Rev. Lett. **120**, 207203 (2018).
[8] Y. Li, P. Gegenwart, and A. A. Tsirlin, J. Phys.: Condens. Matter **32**, 224004 (2020).
[9] D. A. Huse and V. Elser, Phys. Rev. Lett. **60**, 2531 (1988).
[10] M. Yamashita, N. Nakata, Y. Senshu, M. Nagata, H. M. Yamamoto, R. Kato, T. Shibauchi, and Y. Matsuda, Science **328**, 1246 (2010).
[11] S. Yamashita, T. Yamamoto, Y. Nakazawa, M. Tamura, and R. Kato, Nat. Commun. **2**, 275 (2011).
[12] T.-H. Han, J. S. Helton, S. Chu, D. G. Nocera, J. A. Rodriguez-Rivera, C. Broholm, and Y. S. Lee, Nature (London) **492**, 406 (2012).
[13] Y. Shen, Y.-D. Li, H. Wo, Y. Li, S. Shen, B. Pan, Q. Wang, H. C. Walker, P. Steffens, M. Boehm, Y. Hao, D. L. Quintero-Castro, L. W. Harriger, M. D. Frontzek, L. Hao, S. Meng, Q. Zhang, G. Chen, and J. Zhao, Nature (London) **540**, 559 (2016).
[14] Y. Kasahara, T. Ohnishi, Y. Mizukami, O. Tanaka, S. Ma, K. Sugii, N. Kurita, H. Tanaka, J. Nasu, Y. Motome, T. Shibauchi, and Y. Matsuda, Nature (London) **559**, 227 (2018).
[15] J. M. Ni, B. L. Pan, B. Q. Song, Y. Y. Huang, J. Y. Zeng, Y. J. Yu, E. J. Cheng, L. S. Wang, D. Z. Dai, R. Kato, and S. Y. Li, Phys. Rev. Lett. **123**, 247204 (2019).
[16] Z. Zhu, P. A. Maksimov, S. R. White, and A. L. Chernyshev, Phys. Rev. Lett. **119**, 157201 (2017).
[17] I. Kimchi, A. Nahum, and T. Senthil, Phys. Rev. X **8**, 031028 (2018).
[18] T.-H. Han, M. R. Norman, J.-J. Wen, J. A. Rodriguez-Rivera, J. S. Helton, C. Broholm, and Y. S. Lee, Phys. Rev. B **94**, 060409(R) (2016).
[19] P. Czajka, T. Gao, M. Hirschberger, P. Lampen-Kelley, A. Banerjee, J. Yan, D. G. Mandrus, S. E. Nagler, and N. P. Ong, Nat. Phys. **17**, 915 (2021).
[20] W. Liu, Z. Zhang, J. Ji, Y. Liu, J. Li, X. Wang, H. Lei, G. Chen, and Q. Zhang, Chin. Phys. Lett. **35**, 117501 (2018).
[21] M. Baenitz, P. Schlender, J. Sichelschmidt, Y. A. Onykiienko, Z. Zangeneh, K. M. Ranjith, R. Sarkar, L. Hozoi, H. C. Walker, J.-C. Orain, H. Yasuoka, J. van den Brink, H. H. Klauss, D. S. Inosov, and T. Doert, Phys. Rev. B **98**, 220409(R) (2018).
[22] Z. Zhang, X. Ma, J. Li, G. Wang, D. T. Adroja, T. P. Perring, W. Liu, F. Jin, J. Ji, Y. Wang, Y. Kamiya, X. Wang, J. Ma, and Q. Zhang, Phys. Rev. B **103**, 035144 (2021).
[23] B. Schmidt, J. Sichelschmidt, K. M. Ranjith, T. Doert, and M. Baenitz, Phys. Rev. B **103**, 214445 (2021).
[24] K. M. Ranjith, S. Luther, T. Reimann, B. Schmidt, P. Schlender, J. Sichelschmidt, H. Yasuoka, A. M. Strydom, Y. Skourski, J. Wosnitza, H. Kühne, T. Doert, and M. Baenitz, Phys. Rev. B **100**, 224417 (2019).
[25] P.-L. Dai, G. Zhang, Y. Xie, C. Duan, Y. Gao, Z. Zhu, E. Feng, Z. Tao, C.-L. Huang, H. Cao, A. Podlesnyak, G. E. Granroth, M. S. Everett, J. C. Neuefeind, D. Voneshen, S. Wang, G. Tan, E. Morosan, X. Wang, H.-Q. Lin, L. Shu, G. Chen, Y. Guo, X. Lu, and P. Dai, Phys. Rev. X **11**, 021044 (2021).
[26] Z. Zhang, J. Li, M. Xie, W. Zhuo, D. T. Adroja, P. J. Baker, T. G. Perring, A. Zhang, F. Jin, J. Ji, X. Wang, J. Ma, and Q. Zhang, arXiv:2112.07199.
[27] Z. H. Zhu, B. L. Pan, L. P. Nie, J. M. Ni, Y. X. Yang, C. S. Chen, Y. Y. Huang, E. J. Cheng, Y. J. Yu, A. D. Hillier, X. H. Chen, T. Wu, Y. Zhou, S. Y. Li, and L. Shu, arXiv:2112.06523.

[28] See Supplemental Material at http://link.aps.org/supplemental/10.1103/PhysRevB.106.024404 for experimental methods and EDX, powder x-ray diffraction, additional magnetization, and additional specific heat data.
[29] P. A. Goddard, J. Singleton, P. Sengupta, R. D. McDonald, T. Lancaster, S. J. Blundell, F. L. Pratt, S. Cox, N. Harrison, J. L. Manson, H. I. Southerland, and J. A. Schlueter, New J. Phys. **10**, 083025 (2008).
[30] C. A. Pocs, P. E. Siegfried, J. Xing, A. S. Sefat, M. Hermele, B. Normand, and M. Lee, Phys. Rev. Research **3**, 043202 (2021).
[31] Z. Zhang, J. Li, W. Liu, Z. Zhang, J. Ji, F. Jin, R. Chen, J. Wang, X. Wang, J. Ma, and Q. Zhang, Phys. Rev. B **103**, 184419 (2021).
[32] R. L. Carlin, *Magnetochemistry* (Springer, Berlin, 1986).
[33] Y. Li, H. Liao, Z. Zhang, S. Li, F. Jin, L. Ling, L. Zhang, Y. Zou, L. Pi, Z. Yang, J. Wang, Z. Wu, and Q. Zhang, Sci. Rep. **5**, 16419 (2015).
[34] S. Hernández, R. Cuscó, D. Pastor, L. Artús, K. P. O'Donnell, R. W. Martin, I. M. Watson, Y. Nanishi, and E. Calleja, J. Appl. Phys. **98**, 013511 (2005).
[35] S.-H. Su, W.-T. Hsu, C.-L. Hsu, C.-H. Chen, M.-H. Chiu, Y.-C. Lin, W.-H. Chang, K. Suenaga, J.-H. He, and L.-J. Li, Front. Energy Res. **2**, 27 (2014).
[36] J. Spalek, A. Lewicki, Z. Tarnawski, J. K. Furdyna, R. R. Galazka, and Z. Obuszko, Phys. Rev. B **33**, 3407 (1986).
[37] J. D. Rinehart and J. R. Long, Chem. Sci. **2**, 2078 (2011).
[38] Z. Zangeneh, S. Avdoshenko, J. Van Den Brink, and L. Hozoi, Phys. Rev. B **100**, 174436 (2019).
[39] R. Bag, M. Ennis, C. Liu, S. E. Dissanayake, Z. Shi, J. Liu, L. Balents, and S. Haravifard, Phys. Rev. B **104**, L220403 (2021).
[40] J. G. Rau and M. J. P. Gingras, Phys. Rev. B **98**, 054408 (2018).
[41] S. Nakatsuji, Y. Nambu, K. Onuma, S. Jonas, C. Broholm, and Y. Maeno, J. Phys.: Condens. Matter **19**, 145232 (2007).
[42] C. Balz, B. Lake, A. T. M. Nazmul Islam, Y. Singh, J. A. Rodriguez-Rivera, T. Guidi, E. M. Wheeler, G. G. Simeoni, and H. Ryll, Phys. Rev. B **95**, 174414 (2017).
[43] R. Rawl, L. Ge, H. Agrawal, Y. Kamiya, C. R. Dela Cruz, N. P. Butch, X. F. Sun, M. Lee, E. S. Choi, J. Oitmaa, C. D. Batista, M. Mourigal, H. D. Zhou, and J. Ma, Phys. Rev. B **95**, 060412(R) (2017).
[44] A. P. Ramirez, R. Jager-Waldau, and T. Siegrist, Phys. Rev. B **43**, 10461 (1991).
[45] Z. Ma, Z.-Y. Dong, S. Wu, Y. Zhu, S. Bao, Z. Cai, W. Wang, Y. Shangguan, J. Wang, K. Ran, D. Yu, G. Deng, R. A. Mole, H.-F. Li, S.-L. Yu, J.-X. Li, and J. Wen, Phys. Rev. B **102**, 224415 (2020).
[46] Y. Okamoto, M. Nohara, H. Aruga-Katori, and H. Takagi, Phys. Rev. Lett. **99**, 137207 (2007).
[47] A. P. Ramirez, G. P. Espinosa, and A. S. Cooper, Phys. Rev. B **45**, 2505 (1992).
[48] T. Furukawa, K. Miyagawa, T. Itou, M. Ito, H. Taniguchi, M. Saito, S. Iguchi, T. Sasaki, and K. Kanoda, Phys. Rev. Lett. **115**, 077001 (2015).
[49] R. R. P. Singh, Phys. Rev. Lett. **104**, 177203 (2010).
[50] H. Kawamura and K. Uematsu, J. Phys.: Condens. Matter **31**, 504003 (2019).
[51] R. D. Shannon, Acta Crystallogr., Sect. A **32**, 751 (1976).
[52] P. Schiffer and I. Daruka, Phys. Rev. B **56**, 13712 (1997).
[53] A. P. Ramirez, B. Hessen, and M. Winklemann, Phys. Rev. Lett. **84**, 2957 (2000).
[54] S. E. Nikitin, T. Xie, A. Podlesnyak, and I. A. Zaliznyak, Phys. Rev. B **101**, 245150 (2020).
[55] E. Häußler, J. Sichelschmidt, M. Baenitz, E. C. Andrade, M. Vojta, and T. Doert, Phys. Rev. Materials **6**, 46201 (2022).